ADVANCED MATERIALS
www.advmat.de

Visualizing the Anomalous Charge Density Wave States in Graphene/$NbSe_2$ Heterostructures

Yu Chen, Lishu Wu, Hai Xu, Chunxiao Cong, Si Li, Shun Feng, Hongbo Zhang, Chenji Zou, Jingzhi Shang, Shengyuan A. Yang, Kian Ping Loh, Wei Huang,* and Ting Yu**

Metallic layered transition metal dichalcogenides (TMDs) host collective many-body interactions, including the competing superconducting and charge density wave (CDW) states. Graphene is widely employed as a heteroepitaxial substrate for the growth of TMD layers and as an ohmic contact, where the graphene/TMD heterostructure is naturally formed. The presence of graphene can unpredictably influence the CDW order in 2D CDW conductors. This work reports the CDW transitions of 2H-$NbSe_2$ layers in graphene/$NbSe_2$ heterostructures. The evolution of Raman spectra demonstrates that the CDW phase transition temperatures (T_{CDW}) of $NbSe_2$ are dramatically decreased when capped by graphene. The induced anomalous short-range CDW state is confirmed by scanning tunneling microscopy measurements. The findings propose a new criterion to determine the T_{CDW} through monitoring the line shape of the A_{1g} mode. Meanwhile, the 2D band is also discovered as an indicator to observe the CDW transitions. First-principles calculations imply that interfacial electron doping suppresses the CDW states by impeding the lattice distortion of 2H-$NbSe_2$. The extraordinary random CDW lattice suggests deep insight into the formation mechanism of many collective electronic states and possesses great potential in modulating multifunctional devices.

The successful isolation of graphene from graphite has intrigued extensive exploration of the analogous layered transition metal dichalcogenides (TMDs) in solid-state physics because of their flexible properties and feasible revolution in modern technology.[1,2] Apart from the well-studied 2D semiconducting MX_2 (e.g., M = Mo, W; X = S, Se), atomically thin metallic TMDs have a variety of prevailing collective many-body phenomena, including the competing charge density wave (CDW) orders and superconductivity.[3–5] Understanding the electronic modulations of CDW states and the associated spontaneous periodic lattice distortions is significantly required to unveil the mechanism of coexisting phase diagram in low dimensions.[6,7]

The layered TMD niobium diselenide (2H-$NbSe_2$), which is a hole metal at room temperature,[8] has recently gathered tremendous attention as it provides an essential prototype for the exploration

Dr. Y. Chen, Prof. J. Shang, Prof. W. Huang
Shaanxi Institute of Flexible Electronics (SIFE)
Northwestern Polytechnical University (NPU)
Xi'an 710129, China
E-mail: iamwhuang@nwpu.edu.cn
Dr. Y. Chen, L. Wu, Dr. S. Feng, H. Zhang, Dr. C. Zou, Prof. J. Shang, Prof. T. Yu
Division of Physics and Applied Physics
School of Physical and Mathematical Sciences
Nanyang Technological University
Singapore 637371, Singapore
E-mail: yuting@ntu.edu.sg
Prof. H. Xu, Prof. K. P. Loh
Department of Chemistry
National University of Singapore
Singapore 117543, Singapore
Prof. H. Xu
Changchun Institute of Optics
Fine Mechanics and Physics
Chinese Academy of Science
Changchun 130033, China
The ORCID identification number(s) for the author(s) of this article can be found under https://doi.org/10.1002/adma.202003746.
Prof. H. Xu
Center of Materials Science and Optoelectronics Engineering
University of Chinese Academy of Sciences
Beijing 100040, China
Prof. C. Cong
State Key Laboratory of ASIC and System
School of Information Science and Technology
Fudan University
Shanghai 200433, China
E-mail: cxcong@fudan.edu.cn
Prof. C. Cong
Academy for Engineering and Technology
Fudan University
Shanghai 200433, China
Dr. S. Li, Prof. S. A. Yang
Research Laboratory for Quantum Materials
Singapore University of Technology and Design
Singapore 487372, Singapore
Prof. W. Huang
Key Laboratory of Flexible Electronics (KLOFE) & Institute of Advanced Materials (IAM)
Nanjing Tech University (NanjingTech)
Nanjing 211800, China

DOI: 10.1002/adma.202003746

of the collective many-body electronic phases.[9] Bulk 2H-$NbSe_2$ undergoes a second-order phase transition from metal state into incommensurate CDW state at 33 K, and superconductivity state appears when further decreasing the temperature below 7.2 K.[10] The successful fabrication of monolayer and few-layer 2H-$NbSe_2$ by mechanical exfoliation,[6] molecular beam epitaxy (MBE),[11] and chemical vapor deposition (CVD)[12] methods has unraveled the extraordinary changes in these electronic states with the layer thickness. It is believed that the CDW instability in 2H-$NbSe_2$ originates from the strong electron-phonon coupling.[13–15] However, there arises the discrepancy of thickness-dependent CDW phase transition temperature. Specifically, Xi et al. reported a dramatically enhanced CDW transition temperature (T_{CDW}) in mechanical exfoliated monolayer 2H-$NbSe_2$.[6] Ugeda et al. successfully synthesized monolayer 2H-$NbSe_2$ films on epitaxial bilayer graphene via MBE, but observed a lower CDW phase transition temperature.[11] Meanwhile, the desire for wafer-scale and high quality of 2H-$NbSe_2$ has lately promoted the growth in production of thin films using prevalent MBE technique due to its precise controllability in thickness.[11,16,17] Graphene has also been discovered as high transparent electrode on 2D materials to show ohmic-like characteristics at room temperature, which becomes increasingly popular for efficient contacts and highly conducting interconnects in advanced electronic circuits.[18–20] Furthermore, the fragile ultrathin 2H-$NbSe_2$ sheets are often protected by covering hexagonal boron nitride (h-BN), graphene or selenium layers in most studies.[21–23] Conversely, these van der Waals coupled heterostructures could straightly give rise to various interactions at the interface including charge transfer[24] and band structure modulation,[25,26] which may have great effects on the electronic instabilities. For instance, Li et al. discovered an increased CDW phase transition temperature in 1T-$TiSe_2$ flakes by encapsulation with h-BN films.[27] Although the single layer graphene is believed to play a role, the studies on the CDW orders in metallic 2D TMDs affected by the neighboring graphene layer is still lacking.

Direct characterization by in situ Raman spectroscopy and scanning tunneling microscopy/spectroscopy (STM/STS) can deliver a precise presence of the complex CDW orders and facilitate a better investigation of the interplay between graphene and CDW materials. In this work, the heterostructures of stacking single layer graphene on 2H-$NbSe_2$ layers have been systematically investigated by using diverse techniques. First, the CDW phase transition temperatures are clearly identified through in situ temperature dependent Raman spectroscopy. By comparison, the T_{CDW} of 2H-$NbSe_2$ is significantly lowered when covering a single layer graphene. Our work offers a straightforward method to monitor the CDW transitions in 2H-$NbSe_2$-exploiting the linewidth of A_{1g} mode, which is much easier to realize than the previous low-frequency amplitude peak. Then, STM/STS is employed to identify the suppressed short-range CDW orders for the first time and provides evidence of interlayer charge transfer within graphene/$NbSe_2$ heterostructures. Theoretical modeling of the heterostructures reveals that the electron transfer from the single layer graphene is accountable for the suppression effect. The discoveries remind us that we should carefully take into account the interface effects when we investigate the electronic instabilities of 2D TMDs. These observations in graphene/$NbSe_2$ heterostructures develop a direct and nondestructive routine to explore the proximity effect-induced tuning of CDW order transition, and further enrich the basic understanding of CDW formation mechanism in 2H-$NbSe_2$.

2H-$NbSe_2$ is one of the most representative metallic TMDs with both CDW and superconductivity orders. It consists of hexagonal layers of niobium (Nb) atoms that are sandwiched between selenium (Se) layers in a trigonal prismatic crystal structure. Particularly, the hexagonal Nb plane plays a vital part in the formation of CDW as the atomic displacements create a $3a_0 \times 3a_0$ incommensurate CDW supercell with clusters of Nb atoms.[28] **Figure 1**a illustrates the schematic of the fabricated graphene/$NbSe_2$ heterostructures via dry transfer method. First of all, monolayer graphene was mechanically exfoliated

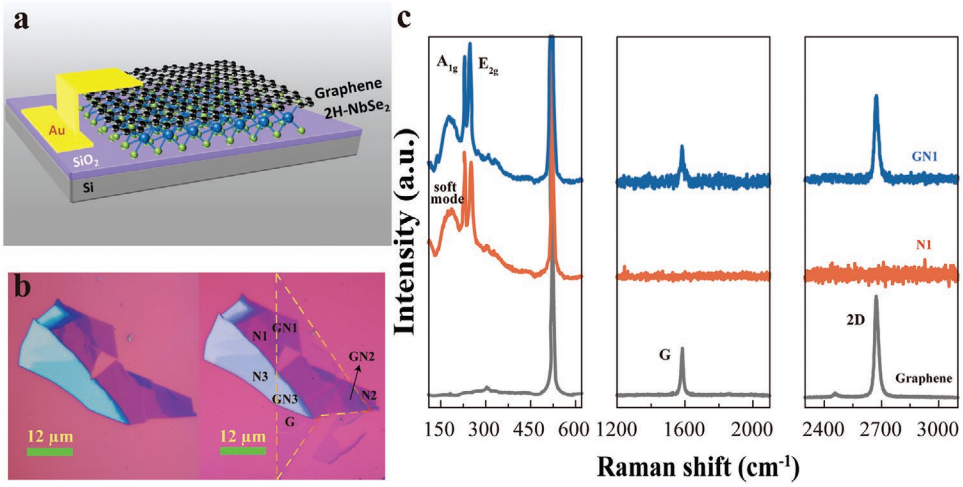

Figure 1. Graphene/$NbSe_2$ heterostructures on SiO_2/Si substrate. a) Schematic of the fabricated graphene/$NbSe_2$ heterostructures. b) Optical image of the samples. The top single layer graphene is enclosed by the yellow dotted lines. The pristine 2H-$NbSe_2$ with different thicknesses are labelled by N1, N2, and N3, and their heterostructures are correspondingly named as GN1, GN2, and GN3, respectively. c) Nonpolarized Raman spectra from pristine graphene, N1, and GN1 at room temperature.

onto the PDMS/glass, followed by the identification of thickness through the optical contrast and Raman spectra. Subsequently, the 2H-$NbSe_2$ flakes with different thicknesses were also prepared through mechanical exfoliation method and then transferred onto SiO_2/Si substrate. The assembly of monolayer graphene/$NbSe_2$ heterostructures together with the dry transfer process was conducted under the optical microscope equipped with the micromanipulator (see the Experimental Section in the Supporting Information). The optical image of the samples is shown in Figure 1b. Note that the $NbSe_2$ samples with different thicknesses, N1, N2, and N3 are partially covered by monolayer graphene (marked as GN1, GN2, and GN3), so that the comparison between the covered and corresponding uncovered samples can be made directly. The thickness and uniformity of the 2H-$NbSe_2$ flake were characterized by topological atomic force microscope (AFM) scans. The height profile shows that a thickness of the thinnest $NbSe_2$ layer, which is indicated as N1 in Figure 1b, is ≈4.2 nm (Figure S1, Supporting Information).

As a representative, the non-polarized Raman spectra of graphene/$NbSe_2$ heterostructure at room temperature are shown in Figure 1c, where the gray, orange and blue curves represent the pristine graphene, $NbSe_2$ layer (N1) and their heterostructure (GN1). Two major Raman peaks centered at around 1580 and 2670 cm^{-1} are observed in pure graphene layer, which are assigned to the G and 2D bands, respectively. The sharp and symmetric 2D band combined with a large intensity ratio of 2D and G peaks indicates that the graphene is indeed monolayer.[29] For the pristine $NbSe_2$ layer (N1), the Raman spectrum is dominated by sharp peaks of A_{1g} mode (out-of-plane vibrations) at about 230 cm^{-1} and E_{2g} mode (in-plane vibrations) at 250 cm^{-1}.[30] Below 200 cm^{-1}, a broad soft mode is obviously found to be centered at 180 cm^{-1} with the full width at half-maximum (FWHM) of approximate 50 cm^{-1}, which is associated with a second-order scattering process.[6] When N1 is covered by graphene, the Raman spectrum exhibits "sum" peak features of N1 and graphene, which is a normal signature of the heterostructures.

To determine the exact CDW transition temperatures in our graphene/$NbSe_2$ system, the temperature dependent variations in Raman spectra were utilized due to the strong optical signatures of CDW phase transitions. We fitted the prominent Raman peaks of both 2H-$NbSe_2$ and graphene by Lorentz function. As apparent from **Figure 2**a, the FWHM of A_{1g} mode from N1 initially increases upon cooling and reaches its maximum when the temperature comes close to 150 K. However, the linewidth in reverse decreases with the continuative cooling. Notably, the critical temperature of 150 K coincides with the CDW transition temperature determined by the soft mode (Supporting Information). Figure 2b shows the FWHM of A_{1g} mode taken from the capped 2H-$NbSe_2$ layer of GN1. Interestingly, the maximum linewidth takes place at the temperature of 120 K, which is also in agreement with the evolution of soft mode, suggesting a lower CDW phase transition temperature at about 120 K when the single layer graphene is introduced

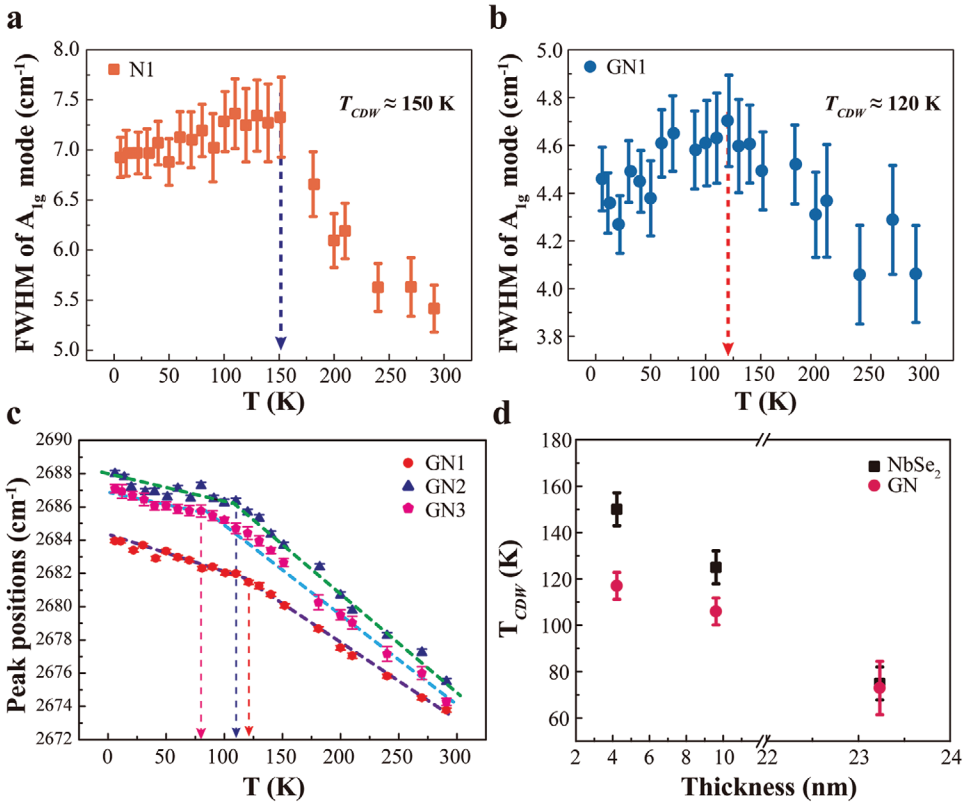

Figure 2. CDW transition temperatures of graphene/$NbSe_2$ heterostructures. a,b)The linewidth of A_{1g} mode at various temperatures from the thinnest part of N1 (a) and the corresponding heterostructures of GN1 (b). c) Positions of graphene 2D band as a function of temperature. d) The CDW transition temperatures from the pristine and capped 2H-$NbSe_2$ films. The error bars are estimated from the fitting uncertainties.

onto the thinnest 2H-$NbSe_2$ film indicated as GN1 in this work. It seems that the CDW order in 2H-$NbSe_2$ film is considerably suppressed by the top graphene layer. It is well known that the electron-phonon coupling plays a significant role in contribution to the phonon linewidth.[31] Our results reveal that the A_{1g} mode of 2H-$NbSe_2$ couples more tightly with electrons, and the alteration in the A_{1g} linewidth is a consequence of the CDW states related electron-phonon coupling. Indeed, a straightforward and accurate approach is established to experimentally determine the T_{CDW} of 2H-$NbSe_2$. Moreover, the CDW transition temperatures for other parts with different thicknesses in our graphene/$NbSe_2$ heterostructures were identified in the same manner (Figures S2 and S3, Supporting Information). The uncovered 2H-$NbSe_2$ layers always have higher T_{CDW} than those of the corresponding heterostructures, although all the CDW phase transition temperatures shift towards lower values upon increasing the thickness of 2H-$NbSe_2$ layer. The thickness dependent T_{CDW} realizes that the major mechanism for CDW states in atomically thin 2H-$NbSe_2$ is most likely attributed to the strong electron-phonon coupling.[6]

For the single-layer graphene, the fitting results of 2D band are summarized in Figure 2c due to the weak features of G band. The frequencies of 2D band follow a drastically redshift with the increasing temperature, arising from the anharmonic terms in the lattice potential energy.[32] Importantly, we found that the evolution of peak frequency as a function of temperature was not a linear progress, exhibiting evident kinks at around 120, 110, and 80 K for GN1, GN2, and GN3, respectively. All these temperatures at which the kinks occur are well coincident with the CDW transition temperatures. Since the positions of 2D Raman peak can be modified by electrical doping through electron-phonon coupling,[33] the carrier density of single layer graphene may be modulated by the charge transfer between the heterostructures. The CDW transition temperatures from the various areas of heterostructures extracted using different criteria are listed in Table S1 (Supporting Information) and described in Figure 2d. The disparity of T_{CDW} between the intrinsic and capped 2H-$NbSe_2$ films becomes smaller and smaller with increasing the thickness of 2H-$NbSe_2$ layers, and almost vanishes in thick samples.

The low temperature STM measurements were also carried out to analyze the CDW orders and interlayer coupling in the graphene/$NbSe_2$ systems. **Figure 3** illustrates the STM/STS images with resolution of atomic level taken on the graphene/$NbSe_2$ heterostructures at a temperature of 77.8 K. Figure 3a shows a standard STM and corresponding 2D-Fouirer (FT) transform images at an isolated bulk 2H-$NbSe_2$. It exhibits a typical metal phase at low temperature, in which the surface selenium atoms form a hexagonal lattice to display a 1×1 surface with lattice spacing of 3.44 Å. Although some Se defects or interstitials are visible, the density of such defects is very low, which indicates a best crystals preparation. When we move STM tip to image the thick area of 2H-$NbSe_2$ (N3 labeled in Figure 1b), there appears a perfect long-range incommensurate (3×3) charge-ordered CDW phase, as shown in Figure 3b. Here, it is clearly confirmed that a CDW phase transition happens depending on the flake thickness, which is a good agreement with the previous observation that CDW phase transition temperatures shift towards lower values upon increasing the thickness of 2H-$NbSe_2$ layers.

Moreover, for the purpose of exploring the effect of single layer graphene, we have imaged the combined junction between the pure graphene layer and the graphene/$NbSe_2$ heterostructure (marked as G and GN3 areas in Figure 1b). After stacking a single layer graphene on the 2H-$NbSe_2$ flake, the atom-resolved STM images were taken at GN3 area, where the thickness of 2H-$NbSe_2$ is the same as N3 area. Figure 3c is a topographic image of graphene/$NbSe_2$ heterostructure. The graphene domain and graphene/$NbSe_2$ heterostructure domain are separated by an obvious grain boundary, which indicates that the fabricated graphene/$NbSe_2$ heterostructure is of very high quality. In Figure 3d, the underneath 2H-$NbSe_2$ flake of GN3 area was imaged unambiguously after changing the tunneling condition. In contrast to the 2H-$NbSe_2$ flake of N3 area, the long-range ordered CDW state of 2H-$NbSe_2$ were broken into many short-range ordered patches after introducing the graphene top layer. The random CDW domains incredibly resemble the phenomena that were observed in 2H-$NbSe_2$ crystals intercalated with metal atoms.[34] The results of STM measurements confirm that the CDW phase transition temperature was lowered and the CDW phase coherence was suppressed after covering a graphene layer. Figure 3e shows a perfect hexagonal atomic structure of the top layer graphene from GN3 area. The STS dI/dV spectrum taken on the top graphene layer is shown in Figure 3f. A gap-like feature was observed in the tunneling conductance spectrum, leading to the asymmetry of spectrum about the Femi energy (E_F). This local conductance minimum can be attributed to the inelastic tunneling to the Dirac point (E_D) of graphene, which is also a minimum in the density of states, and has been identified as the Dirac point.[35–38] Remarkably, the dI/dV spectrum exhibits the Dirac point of top graphene layer shifted to a positive value, which agrees well with the previous reports of single layer graphene on negative gate voltage.[35,36] Such Dirac point located at approximately +0.3 V unambiguously manifests a strong p-type doping by the bottom 2H-$NbSe_2$ layer. In consequence, it seems that the interplay of charge transfer occurred between the single layer graphene and 2H-$NbSe_2$ layers, which has a significant impact on the CDW instabilities.

The prominent suppression of CDW orders observed in our experiments may result from multiple factors, such as the charge transfer or the perpendicular dipole fields in the heterostructure system, whereby the dimensionless electron-phonon interaction strength (i.e., electron phonon coupling constant or density of states effect) is being modified. According to the previous first-principles simulations, higher magnitudes of electric field were observed inside thinner graphene/MoS_2 heterostructures (1L MoS_2) rather than thicker ones (3L MoS_2).[39] The effect of the dipole field should mostly affect the layers close to the interface but diminishes for layers away from the interface. In our work, the 9.6-nm-thick 2H-$NbSe_2$ layer (≈12L) still exhibited remarkable decrease in CDW phase transition temperature by 20 K when capped by a single layer graphene. Therefore, the dipole field is not likely to be the main reason for the observed suppression effect. On the other hand, there could be a sizable charge transfer between graphene and $NbSe_2$ due to their different work functions. Work function is an important quantity to describe the surface properties of a material. It plays a vital role in charge transfer at the interfaces when two different

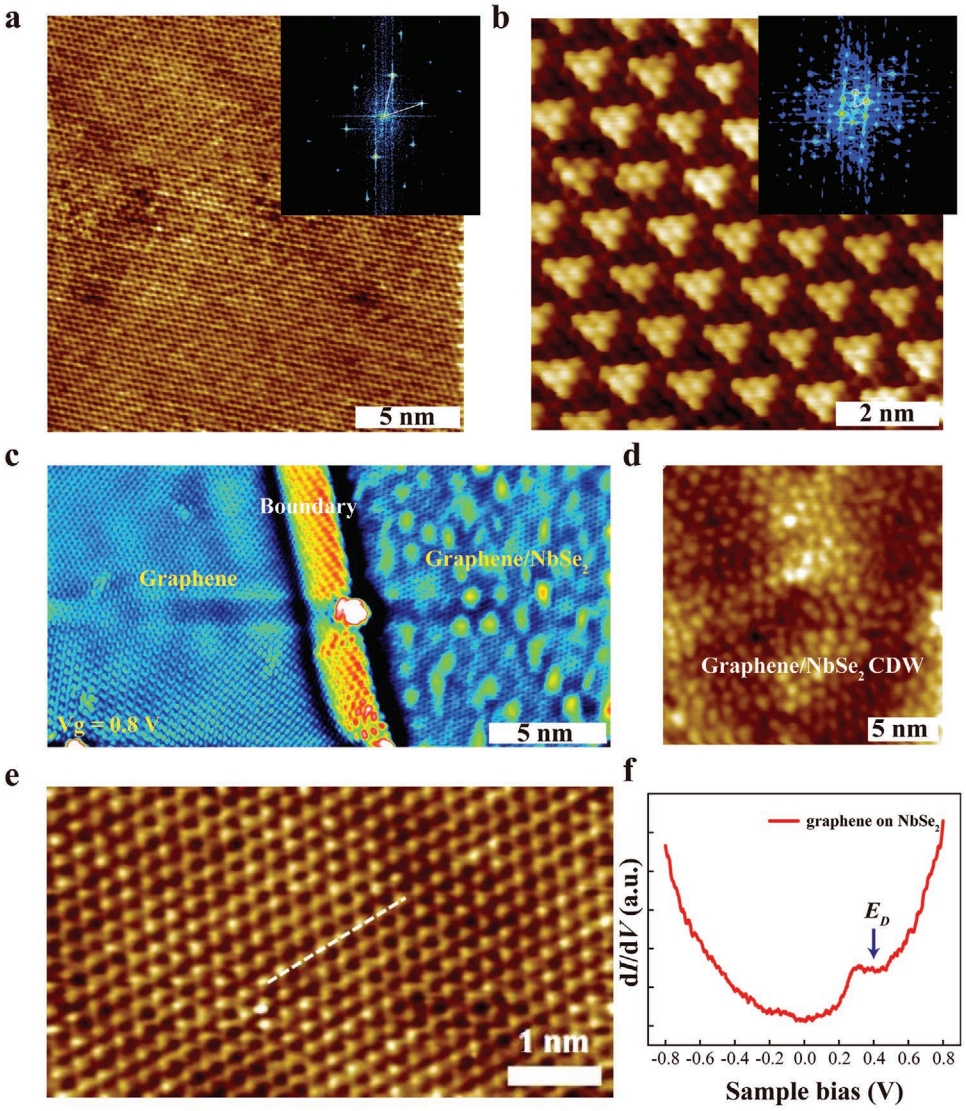

Figure 3. STM/STS images of graphene/2H-$NbSe_2$ heterostructures at the temperature of 77.8 K. a,b) The STM images of the isolated bulk 2H-$NbSe_2$ (a) and the thick 2H-$NbSe_2$ sample indicated as the N3 area (b). The insets show the corresponding 2D-FT transform images. c) STM image from the interface between graphene and GN3 area. d) Close examination of STM image from GN3 area. The random CDW superlattice indicates the distinct suppression of CDW state due to the upper graphene layer. e,f) STM (e) and STS (f) images of the top layer graphene from GN3. The arrow represents the position of the Dirac point E_D. Tunneling parameters: $V = 0.8$ V, $I = 500$ pA, $P = 3.3 \times 10^{-11}$ mbar.

materials are contacting together. In 2D system, charge transfer is the most common interlayer coupling since the layered structure of 2D materials makes it possible to fabricate various heterostructures. The work function of 2H-$NbSe_2$ crystals has been estimated as 5.9 eV experimentally,[40] while the single layer graphene is reported to have the work function in a range of 4.6 eV by previous studies.[41–43] Hence, the electrons are more likely to transfer from graphene to 2H-$NbSe_2$ layers when TMD is covered by a proximal graphene.

To verify the direction of charge transfer in our heterostructures, the frequencies of graphene Raman peaks were analyzed by Lorentz fitting. It has been well identified in top-gated graphene transistor that the positions of both G band and 2D band are highly sensitive to the electron or hole doping.[44,45] Specifically, the behavior of G band position exhibits blue-shift when the single layer graphene is doped by either holes or electrons, whereas the 2D band softens for electron doping and shows distinct stiffening for hole doping. As a result, the frequencies of 2D band take the responsibility to confirm the charge transfer direction. Figure S4 (Supporting Information) summarizes the 2D band positions from both pure graphene and heterostructures at various temperatures. Obviously, the 2D band of all the heterostructures displays a remarkable blue-shift compared to that of pure single layer graphene, which clearly demonstrates the p-type doping of graphene when stacked on the 2H-$NbSe_2$ layers.

The experimental results presented above provide a strong evidence that the electrons transfer from the top layer graphene to the bottom 2H-$NbSe_2$ layer. To further support our proposed physical picture, we have performed the first-principles

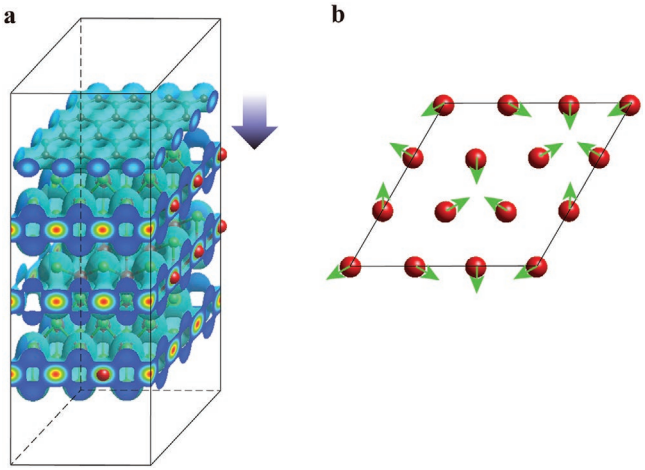

Figure 4. First-principles calculations on graphene/2H-$NbSe_2$ heterostructures. a) Charge transfer between graphene and $NbSe_2$ substrate. The graphene on $NbSe_2$ heterostructure is modeled by taking a graphene monolayer with a 4 × 4 supercell slightly stretched to match the three layers $NbSe_2$ substrate with a 3 × 3 supercell. The isosurface level of charge density is $0.04e/a_0^3$ (a_0: Bohr radius). The arrow represents the charge transfer from the graphene to $NbSe_2$. b) Top view of the CDW lattice distortion of the three layers $NbSe_2$ with a 3 × 3 supercell. The red balls are the Nb ions and the green arrows represent the Nb ions displaced direction, the Se ions are not displayed.

calculations on the charge transfer between graphene and $NbSe_2$ substrate, and its effect on the CDW state. The graphene on $NbSe_2$ heterostructure is modeled by taking a graphene monolayer with a 4 × 4 supercell slightly stretched to match the $NbSe_2$ substrate with a 3 × 3 supercell (which is based on the observed CDW pattern). Here, it should be noted that the strain imposed on the graphene layer (to match the substrate) may influence the charge transfer, as reported in previous works.[46–48] Nevertheless, we find that the small tensile strain on graphene actually increases its work function and hence would lead to underestimation of the amount of charge transfer, compared to the unstrained case. Therefore, our calculation is expected to capture the physics in a qualitative way. Due to computational capability, we model the substrate by three layers of $NbSe_2$. Our calculation shows that there are about 0.1 electrons per supercell transferred from the graphene layer to the $NbSe_2$ substrate, as illustrated in **Figure 4**a. To investigate the effect of the electron transfer on the CDW state, we compare the degrees of lattice distortions associated with CDW for the two cases with and without electron doping in $NbSe_2$. We fully relax the ionic position of $NbSe_2$. Without doping, in a 3 × 3 supercell of $NbSe_2$, the lattice is distorted due to CDW, with the Nb ions displaced as shown in Figure 4b. Here, the Nb–Nb atom distance is changed by about 1.74% compared with the lattice before relaxation. The distortion is alleviated after doping electrons to the structure. For example, when two electrons are doped for a supercell, the lattice distortion in the Nb–Nb distance is reduced to 0.186%. This indicates that the electron transfer has the effect of suppressing the CDW state of $NbSe_2$, which is qualitatively consistent with our experiment results. As a canonical hole metal, the electron doping could dramatically decrease the hole density of 2H-$NbSe_2$, the carrier density and the electronic density of state near the Fermi surface as a consequence modulate the electron–phonon coupling,[8] resulting in the suppression of CDW transitions.

In summary, we investigated and visualized the anomalous CDW states in graphene/$NbSe_2$ heterostructures. Firstly, in situ low temperature Raman spectroscopy demonstrates that the top layer graphene lowers the CDW transition temperature of 2H-$NbSe_2$. For the first time, the STM images exhibit a broken short range CDW order on the capped 2H-$NbSe_2$ layer. First-principles calculations of the CDW orders in graphene/$NbSe_2$ heterostructures indicate that the suppression of CDW states can be attributed to the interlayer charge transfer between the single layer graphene and 2H-$NbSe_2$ layers. Our work suggests a more forthright and versatile method to monitor the CDW transitions in 2H-$NbSe_2$, which could be expanded in analogous CDW conductors. The findings of short-range order CDW states open up a new area to explore the collective electronic phases and enrich the basic understanding of CDW states in multiple heterostructures.

Supporting Information

Supporting Information is available from the Wiley Online Library or from the author.

Acknowledgements

Y.C., L.W., and H.X. contributed equally to this work. This work was mainly supported by the National Key R&D Program of China (Grant No. 2018YFA0703700), the National Natural Science Foundation of China (Nos. 11774170, 61774040), Shanghai Municipal Science and Technology Commission (No. 18JC1410300), the Fudan University-CIOMP Joint Fund (No. FC2018-002), the National Young 1000 Talent Plan of China and Singapore Ministry of Education (MOE) Tier 2 MOE2018-T2-2-072. S.L. and S.A.Y acknowledge the support of Singapore MOE AcRF Tier 2 (Grant No. MOE2017-T2-2-108). W.H. thanks the support of the Natural Science Foundation of Jiangsu Province (BM2012010), Priority Academic Program Development of Jiangsu Higher Education Institutions (YX03001), Ministry of Education of China (IRT1148), Synergetic Innovation Center for Organic Electronics and Information Displays (61136003), the National Natural Science Foundation of China (51173081), and Fundamental Studies of Perovskite Solar Cells (2015CB932200). J.S. appreciates the support of the Fundamental Research Funds for the Central Universities of China, National Natural Science Foundation of China (Grant No. 61904151), Natural Science Foundation of Shaanxi (Grant No. 2020JM-108) and the Joint Research Funds of Department of Science & Technology of Shaanxi Province and Northwestern Polytechnical University (No. 2020GXLH-Z-020).

Conflict of Interest

The authors declare no conflict of interest.

Keywords

2D transition metal dichalcogenides, anomalous charge density wave, graphene/$NbSe_2$ heterostructures, interfacial electron doping, phase transitions

Received: June 1, 2020
Revised: August 29, 2020
Published online: October 1, 2020

[1] Q. H. Wang, K. Kalantar-Zadeh, A. Kis, J. N. Coleman, M. S. Strano, *Nat. Nanotechnol.* **2012**, *7*, 699.
[2] Y. Chen, B. Peng, C. Cong, J. Shang, L. Wu, W. Yang, J. Zhou, P. Yu, H. Zhang, Y. Wang, C. Zou, J. Zhang, S. Liu, Q. Xiong, H. Shao, Z. Liu, H. Zhang, W. Huang, T. Yu, *Adv. Mater.* **2019**, *31*, 1804979.
[3] W. Fu, Y. Chen, J. Lin, X. Wang, Q. Zeng, J. Zhou, L. Zheng, H. Wang, Y. He, H. He, Q. Fu, K. Suenaga, T. Yu, Z. Liu, *Chem. Mater.* **2016**, *28*, 7613.
[4] C. Zhu, Y. Chen, F. Liu, S. Zheng, X. Li, A. Chaturvedi, J. Zhou, Q. Fu, Y. He, Q. Zeng, *ACS Nano* **2018**, *12*, 11203.
[5] W. Fu, J. Qiao, X. Zhao, Y. Chen, D. Fu, W. Yu, K. Leng, P. Song, Z. Chen, T. Yu, S. J. Pennycook, S. Y. Quek, K. P. Loh, *ACS Nano* **2020**, *14*, 3917.
[6] X. Xi, L. Zhao, Z. Wang, H. Berger, L. Forró, J. Shan, K. F. Mak, *Nat. Nanotechnol.* **2015**, *10*, 765.
[7] H. Wang, Y. Chen, M. Duchamp, Q. Zeng, X. Wang, S. H. Tsang, H. Li, L. Jing, T. Yu, E. H. T. Teo, Z. Liu, *Adv. Mater.* **2018**, *30*, 1704382.
[8] X. Xi, H. Berger, L. Forró, J. Shan, K. F. Mak, *Phys. Rev. Lett.* **2016**, *117*, 106801.
[9] C.-S. Lian, C. Si, W. Duan, *Nano Lett.* **2018**, *18*, 2924.
[10] J. A. Wilson, F. J. Di Salvo, S. Mahajan, *Adv. Phys.* **2001**, *50*, 1171.
[11] M. M. Ugeda, A. J. Bradley, Y. Zhang, S. Onishi, Y. Chen, W. Ruan, C. Ojeda-Aristizabal, H. Ryu, M. T. Edmonds, H.-Z. Tsai, *Nat. Phys.* **2016**, *12*, 92.
[12] H. Wang, X. Huang, J. Lin, J. Cui, Y. Chen, C. Zhu, F. Liu, Q. Zeng, J. Zhou, P. Yu, *Nat. Commun.* **2017**, *8*, 394.
[13] C. Arguello, E. Rosenthal, E. Andrade, W. Jin, P. Yeh, N. Zaki, S. Jia, R. Cava, R. Fernandes, A. Millis, *Phys. Rev. Lett.* **2015**, *114*, 037001.
[14] F. Weber, S. Rosenkranz, J.-P. Castellan, R. Osborn, R. Hott, R. Heid, K.-P. Bohnen, T. Egami, A. Said, D. Reznik, *Phys. Rev. Lett.* **2011**, *107*, 107403.
[15] T. Valla, A. Fedorov, P. Johnson, P. Glans, C. McGuinness, K. Smith, E. Andrei, H. Berger, *Phys. Rev. Lett.* **2004**, *92*, 086401.
[16] Y. Nakata, K. Sugawara, S. Ichinokura, Y. Okada, T. Hitosugi, T. Koretsune, K. Ueno, S. Hasegawa, T. Takahashi, T. Sato, *npj 2D Mater. Appl.* **2018**, *2*, 12.
[17] T. Hotta, T. Tokuda, S. Zhao, K. Watanabe, T. Taniguchi, H. Shinohara, R. Kitaura, *Appl. Phys. Lett.* **2016**, *109*, 133101.
[18] S. Bertolazzi, D. Krasnozhon, A. Kis, *ACS Nano* **2013**, *7*, 3246.
[19] Y. Liu, H. Wu, H.-C. Cheng, S. Yang, E. Zhu, Q. He, M. Ding, D. Li, J. Guo, N. O. Weiss, *Nano Lett.* **2015**, *15*, 3030.
[20] Z. Wang, I. Gutiérrez-Lezama, N. Ubrig, M. Kroner, M. Gibertini, T. Taniguchi, K. Watanabe, A. Imamoğlu, E. Giannini, A. F. Morpurgo, *Nat. Commun.* **2018**, *9*, 2516.
[21] R. He, J. van Baren, J. A. Yan, X. Xi, Z. Ye, G. Ye, I. H. Lu, S. Leong, C. Lui, *2D Mater.* **2016**, *3*, 031008.
[22] A. Tsen, B. Hunt, Y. Kim, Z. Yuan, S. Jia, R. Cava, J. Hone, P. Kim, C. Dean, A. Pasupathy, *Nat. Phys.* **2016**, *12*, 208.
[23] S. Onishi, M. M. Ugeda, Y. Zhang, Y. Chen, C. Ojeda-Aristizabal, H. Ryu, S. K. Mo, Z. Hussain, Z. X. Shen, M. F. Crommie, *Phys. Status Solidi B* **2016**, *253*, 2396.
[24] C. H. Lee, G. H. Lee, A. M. Van Der Zande, W. Chen, Y. Li, M. Han, X. Cui, G. Arefe, C. Nuckolls, T. F. Heinz, *Nat. Nanotechnol.* **2014**, *9*, 676.
[25] B. Hunt, J. Sanchez-Yamagishi, A. Young, M. Yankowitz, B. J. LeRoy, K. Watanabe, T. Taniguchi, P. Moon, M. Koshino, P. Jarillo-Herrero, *Science* **2013**, *340*, 1427.
[26] C. Dean, L. Wang, P. Maher, C. Forsythe, F. Ghahari, Y. Gao, J. Katoch, M. Ishigami, P. Moon, M. Koshino, *Nature* **2013**, *497*, 598.
[27] L. Li, W. Zhao, B. Liu, T. Ren, G. Eda, K. Loh, *Appl. Phys. Lett.* **2016**, *109*, 141902.
[28] C. D. Malliakas, M. G. Kanatzidis, *J. Am. Chem. Soc.* **2013**, *135*, 1719.
[29] Z. Ni, Y. Wang, T. Yu, Z. Shen, *Nano Res.* **2008**, *1*, 273.
[30] Y. Wu, M. An, R. Xiong, J. Shi, Q. Zhang, *J. Phys. D: Appl. Phys.* **2008**, *41*, 175408.
[31] B. Chakraborty, A. Bera, D. Muthu, S. Bhowmick, U. V. Waghmare, A. Sood, *Phys. Rev. B* **2012**, *85*, 161403.
[32] I. Calizo, A. Balandin, W. Bao, F. Miao, C. Lau, *Nano Lett.* **2007**, *7*, 2645.
[33] J. Yan, Y. Zhang, P. Kim, A. Pinczuk, *Phys. Rev. Lett.* **2007**, *98*, 166802.
[34] U. Chatterjee, J. Zhao, M. Iavarone, R. Di Capua, J. Castellan, G. Karapetrov, C. Malliakas, M. G. Kanatzidis, H. Claus, J. Ruff, *Nat. Commun.* **2015**, *6*, 6313.
[35] Y. Zhang, V. W. Brar, F. Wang, C. Girit, Y. Yayon, M. Panlasigui, A. Zettl, M. F. Crommie, *Nat. Phys.* **2008**, *4*, 627.
[36] S. Wickenburg, J. Lu, J. Lischner, H.-Z. Tsai, A. A. Omrani, A. Riss, C. Karrasch, A. Bradley, H. S. Jung, R. Khajeh, *Nat. Commun.* **2016**, *7*, 13553.
[37] J. Chae, H. Yang, H. Baek, J. Ha, Y. Kuk, S. Jung, Y. Song, N. Zhitenev, J. Stroscio, S. Woo, *Int. J. High Speed Electron. Syst.* **2011**, *20*, 205.
[38] P. Dabrowski, M. Rogala, I. Wlasny, Z. Klusek, M. Kopciuszynski, M. Jalochowski, W. Strupinski, J. Baranowski, *Carbon* **2015**, *94*, 214.
[39] L. H. Li, T. Tian, Q. Cai, C.-J. Shih, E. J. Santos, *Nat. Commun.* **2018**, *9*, 1.
[40] T. Shimada, F. S. Ohuchi, B. A. Parkinson, *Jpn. J. Appl. Phys.* **1994**, *33*, 2696.
[41] T. Filleter, K. Emtsev, T. Seyller, R. Bennewitz, *Appl. Phys. Lett.* **2008**, *93*, 133117.
[42] Y. Shi, X. Dong, P. Chen, J. Wang, L.-J. Li, *Phys. Rev. B* **2009**, *79*, 115402.
[43] Y. J. Yu, Y. Zhao, S. Ryu, L. E. Brus, K. S. Kim, P. Kim, *Nano Lett.* **2009**, *9*, 3430.
[44] A. Das, S. Pisana, B. Chakraborty, S. Piscanec, S. Saha, U. Waghmare, K. Novoselov, H. Krishnamurthy, A. Geim, A. Ferrari, *Nat. Nanotechnol.* **2008**, *3*, 210.
[45] M. Kalbac, A. Reina-Cecco, H. Farhat, J. Kong, L. Kavan, M. S. Dresselhaus, *ACS Nano* **2010**, *4*, 6055.
[46] H. Suzuura, T. Ando, *Phys. Rev. B* **2002**, *65*, 235412.
[47] J. L. Manes, *Phys. Rev. B* **2007**, *76*, 045430.
[48] S.-M. Choi, S.-H. Jhi, Y.-W. Son, *Phys. Rev. B* **2010**, *81*, 081407.